SAE International

Electronic and Atomistic Roles of Cordierite Substrate in Sintering of Washcoated Catalysts for Automotive Exhaust Gas Emissions Control: Multi-scale Computational Chemistry Approach based on Ultra-Accelerated Quantum Chemical Molecular Dynamics Method

2012-01-1292
Published
04/16/2012

Akira Miyamoto, Ryo Nagumo, Ai Suzuki, Ryuji Miura, Hideyuki Tsuboi, Nozomu Hatakeyama, Hiromitsu Takaba and Sumio Kozawa
Tohoku Univ.

Athonu Chatterjee and Akira Okada
Corning Inc.

doi:10.4271/2012-01-1292

ABSTRACT

Multi-scale computational chemistry methods based on the ultra-accelerated quantum chemical molecular dynamics (UA-QCMD) are applied to investigate electronic and atomistic roles of cordierite substrate in sintering of washcoated automotive catalysts. It is demonstrated that the UA-QCMD method is effective in performing quantum chemical molecular dynamics calculations of crystals of cordierite, Al_2O_3 and $CeZrO_4$ (hereafter denoted as CZ). It is around 10,000,000 times faster than a conventional first-principles molecular dynamics method based on density-functional theory (DFT). Also, the accuracy of the UA-QCMD method is demonstrated to be as high as that of DFT. On the basis of these confirmations and comparison, we performed extensive quantum chemical molecular dynamics calculations of surfaces of cordierite, Al_2O_3 and CZ, and interfaces of Al_2O_3 and CZ with cordierite at various temperatures. These calculations coupled with mesoscopic sintering simulations have demonstrated that the cordierite surface forms strong bonds with Al_2O_3 and CZ, which was seen to improve significantly the sintering property of washcoated catalysts under various conditions.

INTRODUCTION

The lifetime of a vehicle catalyst is important in maintaining low exhaust gas emissions. Typically, mid-life catalyst durability performance is experimentally examined in engine dynamometer evaluations. In general, such traditional confirmation of catalyst performance is done using many kinds of oils and catalysts in continuous evaluation tests. However, so far, little work has been devoted to theoretical evaluation of catalyst sintering behavior. In our previous papers [1, 2, 3], we have reported the results of an alternative methodology to experimental durability testing schemes. We investigated the thermal durability of supported precious metals, represented as Pt, from micro scale to macro scale. We focused not only microscopically on thermal diffusion dynamics of Pt at high temperatures, but also performed macroscopic long-term, sintering process simulation using a three-dimensional sintering simulator [1, 2, 3]. In the present study we have extended our methodology to investigate electronic and atomistic roles of cordierite substrate in sintering of washcoated catalysts. Although it is well known and well accepted that cordierite has excellent mechanical properties and chemical inertness as a substrate[4, 5, 6, 7], the electronic and atomistic roles of cordierite have not yet been

thoroughly studied [8,9]. In this paper we take a step in this direction.

METHOD

1. ULTRA-ACCELERATED QUANTUM CHEMICAL MOLECULAR DYNAMICS (UA-QCMD) METHOD

The electronic structure calculations in the UA-QCMD have been carried out employing a tight-binding quantum chemical (TBQC) approach implemented in our in-house computer code COLORS that can calculate the energies, charges and bond populations for large-scale systems. The potential functions calculated by Colors are used in the NEW-RYUDO molecular dynamics (MD) code to calculate atomic dynamics based on Newton's equations of motions. When the electronic structures of the system are changed by a considerable change in the geometry, COLORS is used to re-evaluate the potential functions for further molecular dynamics calculations with NEW-RYUDO. Using this scheme, on average a speed-up of 10,000,000 times over DFT of quantum chemical molecular dynamics calculation is realized [2,3,10,11]. The detailed scheme is described below

In COLORS an electronic structure calculation is performed by solving the Schrödinger equation (HC = εSC; H, C, ε, and S refer to the Hamiltonian matrix, eigenvectors, eigenvalues, and overlap integral matrix, respectively) with the diagonalization condition ($C^TSC = I$; I refers to the identity matrix). Simulation is carried out on the basis of Born Oppenheimer approximation. In order to determine the off-diagonal elements of H, H_{rs}, the corrected distance-dependent Wolfsberg-Helmholz formula (Eq. (1)) was used.

$$H_{rs} = \frac{K}{2} S_{rs} \left(H_{rr} + H_{ss} \right) \tag{1}$$

In order to solve the Schrödinger equation in this simulator, parameters for Hamiltonian matrix H are used, which will be explained later. For electronic structure calculations using COLORS, the total energy of a system is obtained by using the following equation,

$$E = \sum_{k=1}^{\text{occ}} n_k \varepsilon_k + \sum_{i=1}^{N} \sum_{j=i+1}^{N} \frac{Z_i Z_j e^2}{r_{ij}} + \sum_{i=1}^{N} \sum_{j=i+1}^{N} E_{ij}^{\text{repul}} \left(r_{ij} \right) \tag{2}$$

where the first, second, and third terms on the right-hand side refer to the molecular orbital (MO) energy, columbic energy, and exchange-repulsion energy, respectively. The first term on the right-hand side of Eq. (2) is rewritten as follows,

$$\sum_{k=1}^{\text{occ}} n_k \varepsilon_k = \sum_{k=1}^{\text{occ}} \sum_{r} n_k \left(C_{kr} \right)^2 H_{rr} + \sum_{k=1}^{\text{occ}} \sum_{r} \sum_{s} n_k C_{kr} C_{ks} H_{rs} \tag{3}$$

where the first and second terms on the right-hand side refer to the mono-atomic contribution to the binding energy and the diatomic contribution to the binding energy, respectively (n_k is the number of electrons occupied in k-th MO). A covalent binding energy calculated from the sum of the second term of Eq. (3) and exchange-repulsion term in Eq. (2) for the pair of A and B atoms is used for the determination of the D_{AB} parameter in the Morse-type 2-body interatomic potential function described as Eq. (4) below,

$$E_{AB} = D_{AB} \left\{ \exp\left[-2\beta_{AB} \left(R_{AB} - R_{AB}^* \right) \right] - 2 \exp\left[-\beta_{AB} \left(R_{AB} - R_{AB}^* \right) \right] \right\} \tag{4}$$

where E_{AB}, D_{AB}, β_{AB}, R_{AB}, and R^*_{AB} refer to the interatomic potential energy between atoms A and B, binding energy between atoms A and B, factor for potential curve, interatomic distance between atoms A and B, and equilibrium interatomic distance between atoms A and B, respectively. Using these potentials determined by the above-mentioned scheme, a classical molecular dynamics (MD) simulation was performed using the NEW-RYUDO system. In this MD simulator, a Verlet algorithm is employed to integrate the equations of motion. The temperature scaling method implemented is similar to the Woodcock algorithm.

2. PARAMETERIZATION OF UA-QCMD SIMULATIONS

In order to set the Hamiltonian matrix H and overlap integral matrix S in our TB-QC simulator which is a part of our UA-QCMD simulator, exponents of a Slater-type atomic orbital (AO), denoted as ζ_r, and valence state ionization potentials (VSIPs) for the 1s AO of H atoms as well the 2s and 2p AOs of O atoms, 3s and 3p AOs of Al atoms, s, p, and d AOs for Pt atoms are necessary. The former parameters are used to calculate the S matrix and H_{rs} in Eq. (1). The latter ones are used for the diagonal element of H (H_{rr} or H_{ss} in Eq.(1)). The relationship between H_{rr} and VSIP of r-th AO of the i-th atom (I^i_r) is described as $H_{rr} = -I^i_r$. In our UA-QCMD simulator, these are represented by the polynomial functions of atomic charges. ζ_r, and H_{rr} are calculated by the polynomial functions of atomic charges described by Eqs. (5) and (6), respectively.

$$\zeta_r = a_0 + \sum_{k=1}^{5} a_k \left(Z_i \right)^k \tag{5}$$

$$H_{rr} = b_0 + \sum_{k=1}^{5} b_k \left(Z_i\right)^k \qquad (6)$$

In Eqs. (5) and (6), Z_i corresponds to the atomic charge on atom i. The parameters of ζ_r, i.e., a_0, a_1, a_2, a_3, a_4, and a_5 in Eq. (5) and of H_{rr}, i.e., b_0, b_1, b_2, b_3, b_4, and b_5 in Eq. (6), were determined by DFT calculations, which are summarized in Tables 1 and 2. The DMol[3] code and CASTEP codes were used for this purpose. The energies werecalculated using the generalized gradient approximation (GGA) with Perdew-Burke-Ernzerhof (PBE) exchange-correlation functional. Since the parameters of UA-QCMD are fitted with the DFT calculations, this means that the papameters include the exchange and correlations effects. Similarly the DFT calculations indicated that the spin non-polarized calculations are applied to Al_2O_3, $CeZrO_2$, cordierite, the QCMD calculations were also done under spin non-polarized conditions. It should also be noted that the parameters used in the present UA-OCMD calculations are for ground state dynamics and thus we did not tune to reproduce the band gaps.

Table 1. Coefficients a_0, a_1, a_2, a_3, a_4, and a_5 used in Eq. (5)**.**

Element	A	a_0	a_1	a_2	a_3	a_4	a_5
O	s	2.8102	2.8049	0.0185	0.0	0.0	0.000
	p	2.4015	1.8261	0.6817	0.0	0.0	0.000
Al	s	2.1081	0.2004	0.0118	-0.0542	0.0190	-0.0015
	p	1.9542	0.2346	-0.0321	0.0150	0.0153	-0.0056
Zr	s	1.8515	0.1890	-0.1017	0.0	0.0	0.0
	p	1.6252	0.0300	0.1604	0.0	0.0	0.0
	d	2.1032	0.1787	-0.1182	0.0	0.0	0.0
Ce	s	1.1165	0.0332	0.0208	0.0041	0.0	0.0
	p	1.0592	0.0010	-0.0127	0.0093	0.0	0.0
	d	1.8519	0.3368	0.0	0.0	0.0	0.0
	f	2.9582	0.3363	0.0	0.0	0.0	0.0
Mg	s	1.7065	0.2458	0.0850	0.0	0.0	0.0
	p	1.5692	0.4548	0.0057	0.0091	0.0074	0.0022
Si	s	2.1316	0.8819	0.0187	0.0	0.0	0.0
	p	1.7827	0.8033	-0.0120	0.0	0.0	0.0

Table 2. Coefficients b_0, b_1, b_2, b_3, b_4, and b_5 used in Eq. (6)**.**

Element	AO	b_0	b_1	b_2	b_3	b_4	b_5
O	s	-18.7345	-8.4328	-1.4510	0.0	0.0	0.0
	p	-10.4895	-8.8159	-1.6244	0.0	0.0	0.0
Al	s	-9.0490	-6.5589	-1.4884	0.5003	0.0000	0.0000
	p	-3.4369	-6.4464	-1.4776	-0.1125	0.0000	0.0000
Zr	s	-7.7241	-3.6068	-0.1052	0.0000	0.0000	0.0000
	p	-1.8668	-1.8209	-0.0082	0.0000	0.0000	0.0000
	d	-2.3610	-4.8165	-0.0512	0.0000	0.0000	0.0000
Ce	s	-2.0303	-3.0428	0.0000	0.0000	0.0000	0.0000
	p	-1.5612	-0.2247	0.0000	0.0000	0.0000	0.0000
	d	-4.4856	-3.2609	0.0000	0.0000	0.0000	0.0000
	f	-5.2818	-3.2663	0.0000	0.0000	0.0000	0.0000
Mg	s	-6.6170	-3.2408	-0.0274	0.0000	0.0000	0.0000
	p	-4.2908	-3.1921	-0.1756	0.0000	0.0000	0.0000
Si	s	-8.0134	-8.2128	-0.7569	0.0000	0.0000	0.0000
	p	-4.5024	-7.5560	-0.7423	0.0000	0.0000	0.0000

3. KINETIC MONTE CARLO MESOSCOPIC SINTERING SIMULATOR, SINTA [1, 2, 3]

Diffusion of supported particles and support particles were simulated by the Kinetic Monte Carlo (KMC) method. During the simulation a diffusion direction is randomly generated while the diffusion length for one KMC step, l, is calculated as $l = (D(r)\ \Delta t)^{1/2}$, where D(r) and Δt are the diffusion coefficient given as a function of particle size and the real-scale diffusion time per KMC step, respectively. Sintering dynamics simulator, SINTA, enables us to incorporate atomic scale characteristics of catalytic materials such as the adsorption energies between Pt and each support. These atomic scale characteristics are strongly related to the diffusion behavior of supported precious metals. The values affecting thermal diffusion can be directly calculated using our tight-binding based quantum chemical calculation program, COLORS. We estimated the activation energy for sintering of the supported metal, E_M, from the calculated adsorption energy of Pt on supports. It was incorporated into the sintering simulator for ascertaining thermal diffusions as expressed in Eq. (7)

$$D_M(r) = D_{M0}\ (2r_M)^{-n} \exp(-E_M/RT) \qquad (7)$$

In Eq. (7) T, R and n denote the absolute temperature, the gas constant and particle size dependent coefficient of diffusion of supported metals or supports. D_{M0} denotes surface diffusion coefficient of supported metals. The KMC simulation proceeds by repeating a sintering event for a pre-

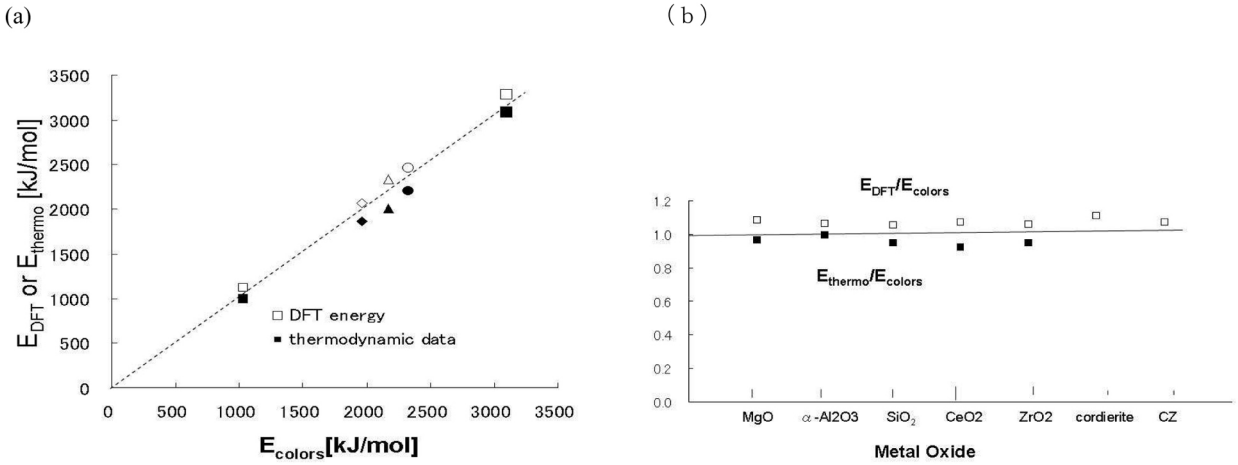

Figure 1. Relationship of binding energy of metal oxide calculated by Colors (E_{colors}) with that by DFT (E_{DFT}) (open symbols) or that by thermodynamics (E_{thermo})(closed symbols) for MgO (square), Al_2O_3, SiO_2 and cordierite, (a). Results of E_{DFT}/ E_{COLORS} (open symbols) and E_{thermo}/E_{COLORS} (closed symbols) are also shown in (b)

determined number of support and precious-metal particles for a pre-determined number of steps. The coordinates calculated by the system are then used to monitor sintering of the supported precious metal particles. For example when the center of a support particle moves within the radius of another support particle, these support particles are changed to one larger particle with the same volume as the sum of two particles. This enables one to compare the characteristics of the sintering process of supported precious metals with experimental results.

RESULTS AND DISCUSSION

1. VALIDATION OF PARAMETERS USED IN UA-QCMD

In order to validate the parameters for Colors, crystalline metal oxides such as Al_2O_3, SiO_2, ZrO_2, CeO_2, MgO, CZ, and cordierite were used. The accuracy of the parameters was ascertained by comparison of atomic charges, atomic orbital populations, bond populations, and total binding energies of the metal oxides between Colors and DFT calculations as shown in Fig. 1. The binding energy calculated by Colors is proportional to that calculated by DFT (Fig. 1a) and their ratio is almost one within an error of around 5% (Fig. 1b). It should also be noted that the ratio of experimental value to the calculated value has a similar error (on an average of around 5%), indicating the validity of the parameters used for Colors calculations.

2. FORMATION DYNAMICS OF AL_2O_3-CORDIERITE INTERFACE

In the experimental washcoat process, support particles such as Al_2O_3 or CZ form bonds with the cordierite substrate surface to produce honey-comb catalyst. It has been demonstrated that the cordierite surface has sufficient bond strength to ensure reliable washcoating [4, 5, 6, 7]. In order to investigate bonding characteristics of Al_2O_3-cordierite interface, UA-QCMD calculations were performed for the model shown in Fig. 2(a) where γ-Al_2O_3(100) plane is in contact with a cordierite(100) plane. Similar calculations performed for different combinations of crystal planes of γ-Al_2O_3 and cordierite yielded similar results. Therefore, detailed calculation results are only presented for the model shown in Fig. 2(a). As shown in Fig. 2(a), initially Al_2O_3 and cordierite are slightly separated to simulate the formation process of the Al_2O_3-cordierite interface. Figures 3 and 4 show snap shots of dynamic change of Al_2O_3 and cordierite during the process. The lattice structure of Al_2O_3 does not change significantly, whereas the cordierite surface changes significantly in comparison to form a stable interface. Almost constant energies of Al-O bonds at different positions relative to the interface during the interface formation process attest to the above observation. On the other hand, the surface geometry of cordierite changes significantly more as shown in Figs. 3 and 4. Larger changes in energies of Mg-O, Al-O, and Si-O bond than that of Al-O bond in Al_2O_3 are consistent with the observation of larger surface structure change in cordierite during the sintering process. This suggests a flexible nature of cordierite surface that aids stable interface formation with Al_2O_3.

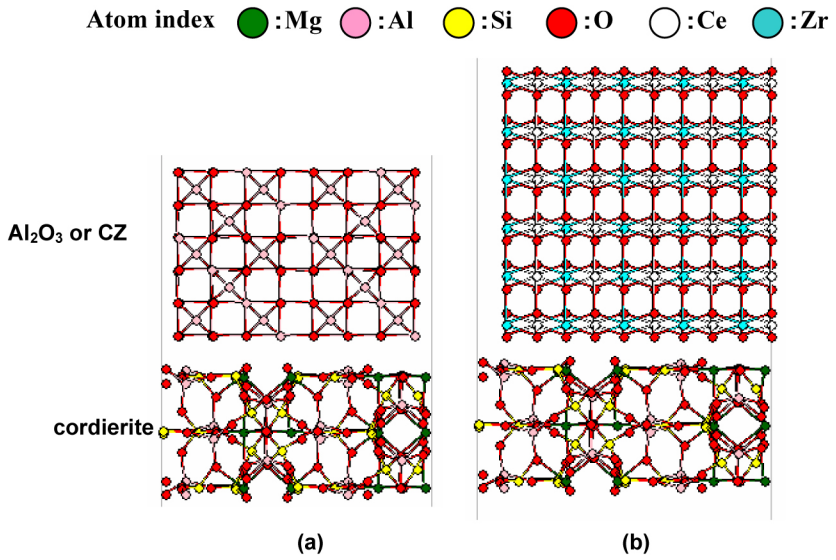

Figure 2. Initial geometry of formation dynamics of Al_2O_3-cordierite interface, (a) and that of CZ-cordierite interface, (b) calculated by UA-QCMD method.

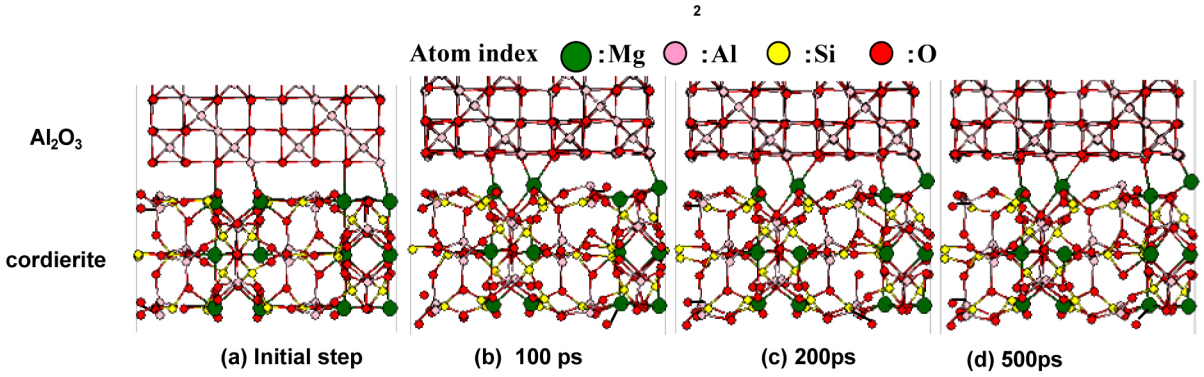

Figure 3. Snapshots of bond formation dynamics of O ion of Al_2O_3 and Mg ion of cordierite at Al_2O_3-cordierite interface at 300 K for various time steps

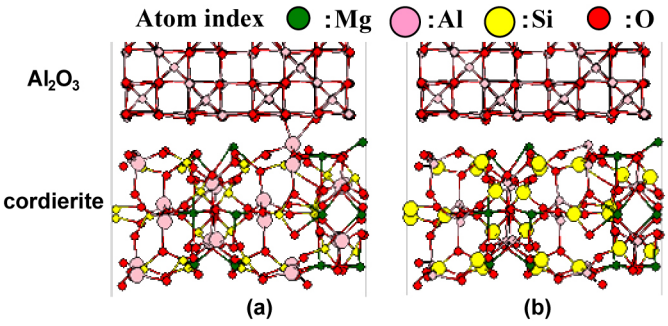

Figure 4. The Al-O bond, (a), and Si-O bond, (b), during Al_2O_3-cordierite interface formation dynamics after 500 ps calculation at 300K.

3. FORMATION DYNAMICS OF CZ-CORDIERITE INTERFACE

As a support material, behavior of CZ is considerably different from Al_2O_3. For example, thermal stability of γ-Al_2O_3 is much higher than that of CZ, while Pt nano particles are more stable on CZ than on γ-Al_2O_3 [1, 2, 3]. Therefore, the formation dynamics of CZ-cordierite interface was simulated for a set-up where initially cubic CZ(100) plane is slightly separated from the surface of cordierite(100) plane. Figure 5 shows snap shots of dynamic change of CZ and cordierite during the sintering process. The geometry of CZ does not seem to change significantly, whereas the cordierite surface changes significantly in comparison. Almost constant energies of Ce-O and Zr-O bonds at different positions relative to the interface during the interface formation process agree with this observation. On the other hand, the surface

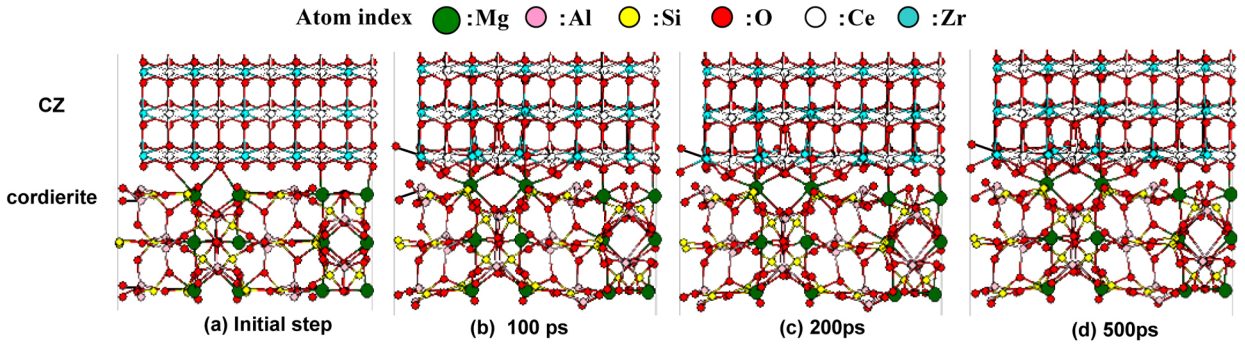

Figure 5. Snapshots of bond formation dynamics of O ion of CZ and Mg ion of cordierite at CZ-cordierite Interface at 300 K for various time steps

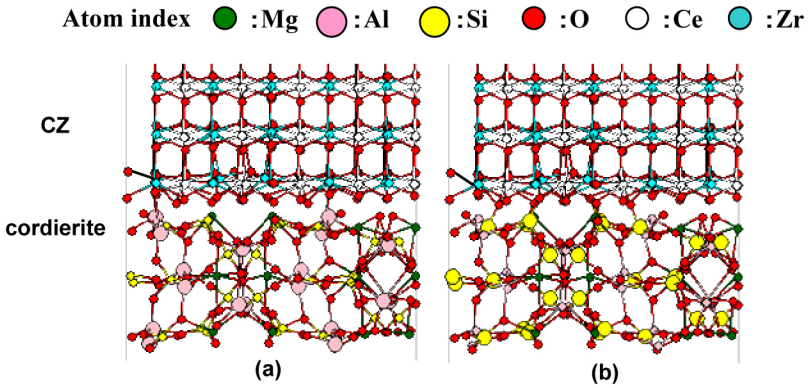

Figure 6. The Al-O bond, (a), and Si-O bond, (b), during CZ-cordierite interface formation dynamics after 500 ps calculation at 300K.

geometry of cordierite changes more than that of CZ as shown in Figs. 5 and 6. In accordance with this observation, the energies of Mg-O, Al-O, and Si-O bonds change significantly more than that of Ce-O or Zr-O bond in CZ. This again suggests a flexible nature of cordierite surface that assists in stable interface formation. It should also be mentioned that this behavior of CZ is similar to that of Al_2O_3, possibly indicating that flexible nature of cordierite surface manifests generally for support materials with entirely different characteristics.

4. DYNAMICS OF AL_2O_3-CORDIERITE AND CZ-CORDIERITE INTERFACE AT VARIOUS TEMPERATURES

Dynamics of atoms at Al_2O_3-cordierite interface at various temperatures were calculated and the energies of various bonds in Al_2O_3 and cordierite are shown in Fig. 7. As shown in Fig. 7a, the energy of Al-O bond at the Al_2O_3-cordierite interface does not change significantly with temperature and Al-O bond at higher temperatures is slightly weaker than that at lower temperatures. Similarly, as shown in Fig 7b, energies of Mg-O, Al-O, or Si-O bond in cordierite at the interface does not change significantly with temperature. Similar results can also be seen for the energies of Al-O, Mg-O, or Si-O bonds between Al_2O_3 and cordierite at different temperatures.

This is consistent with experimental observation [4, 5, 6, 7] that cordierite exhibits excellent characteristics as a substrate for automotive catalysts, which are operated at different (high) temperatures.

Similar results are also observed for CZ-cordierite interface at various temperatures, as shown in Fig. 8. As shown in Fig. 8a, the energies of CeO and Zr-O bond at the CZ-cordierite interface does not change significantly with temperature, the energies at high temperature being slightly weaker than that at lower temperatures. Similarly, as shown in Fig. 8b, energies of Mg-O, Al-O, and Si-O bonds in cordierite at the interface does not change significantly with temperature. Similar results can also be seen for the energies of Al-O, Mg-O, Si-O, Zr-O, or Ce-O bonds between CZ and cordierite at different temperatures. This is also consistent with experimental findings [4, 5, 6, 7].

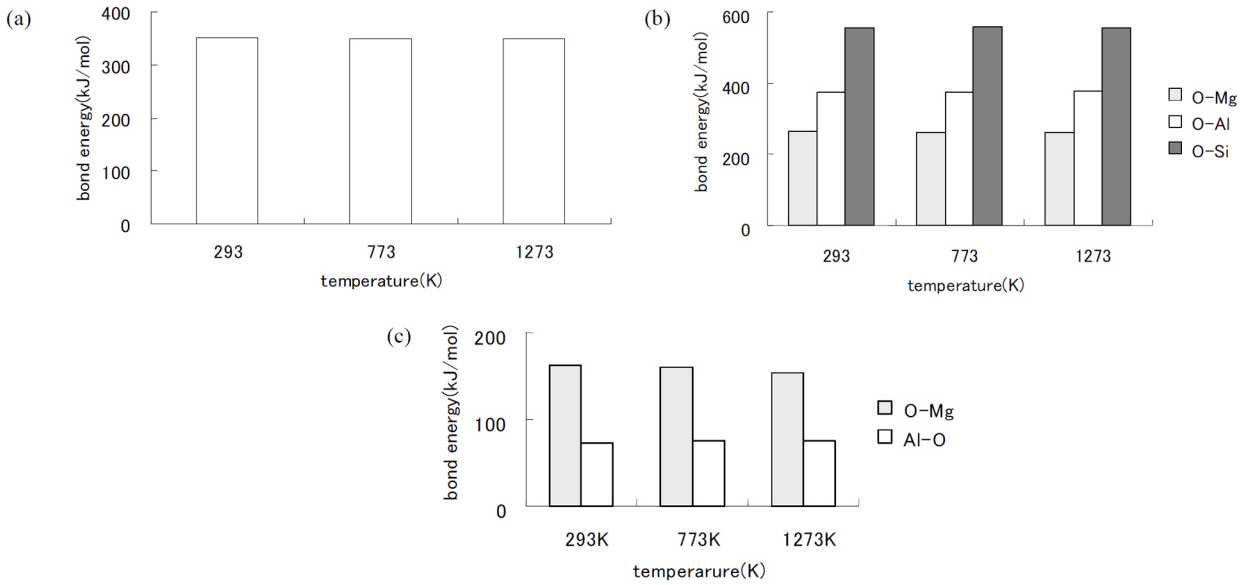

Figure 7. Energy change of Al-O bonds in Al_2O_3,(a), that of Mg-O, Al-O, and Si-O bonds in cordierite,(b), and that of bonds between Al_2O_3 and cordierite, (c), for the Al_2O_3-cordierite interface at various temperatures.

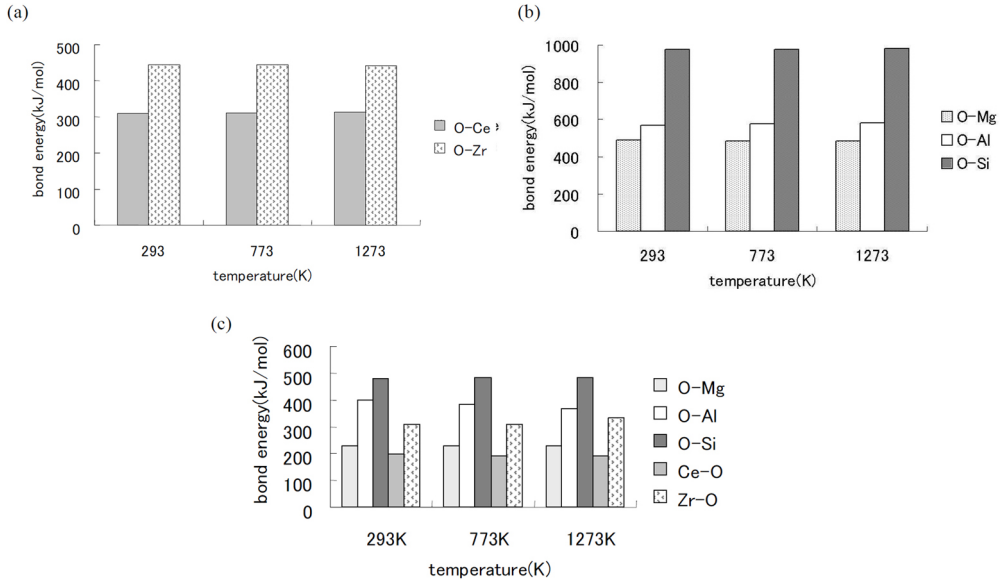

Figure 8. Energy change of Ce-O and Zr-O bonds in CZ, (a), that of Mg-O, Al-O, and Si-O bonds in cordierite, (b), and that of bonds between CZ and cordierite, (c), for the CZ-cordierite interface at various temperatures.

5. BONDING NATURE OF CORDIERITE-SUPPORT INTERFACE

From the calculated bond energies between cordierite and support (CZ and alumina) we can discuss atomistic role of cordierite in forming bonds at the interface at various temperatures. In the cordierite crystal, Si-O or Al-O bond is much stronger than the Mg-O bond. This can be seen in Fig. 7b for Al_2O_3-cordierite interface and Fig. 8b for CZ-cordierite interface. On the other hand, Mg-O bond contributes significantly to the interfacial interaction between Al_2O_3 and cordierite (Fig. 7c). Similar results are also observed for the interaction between CZ and cordierite (Fig. 8). It can also be seen that Ce-O and Zr-O bonds also contribute to the bonding between CZ and cordierite, although the energy of Ce-O or Zr-O bond in CZ does not decrease at the interface. Such a flexible nature of bonding interaction at cordierite-support interface may also be responsible for excellent performances of cordierite as a substrate for automotive catalysts. According to the

calculation results in Figs. 7 and 8 CZ interacts with cordierite more strongly than Al_2O_3. This is probably because binding energy of CZ is weaker than Al_2O_3 and thus more easily deforms than Al_2O_3 to optimize the interface structure.

6. ROLE OF CORDIERITE-SUPPORT INTERACTION IN THE SINTERING BEHAVIOR OF WASHCOATED CZ AND AL_2O_3

In order to investigate the influence of cordierite-support interaction on the sintering behavior of washcoated catalysts, the mesoscopic sintering simulator, SINTA, was applied to simulate sintering dynamics of CZ with and without CZ-cordierite interaction at different temperatures. Since SINTA has been validated [1, 2, 3] to simulate accurately the sintering behavior of Al_2O_3 and CZ, the same parameters were used for sintering of CZ and Al_2O_3 washcoated on cordierite. To investigate the role of the interface interaction in sintering clearly, all of CZ and Al_2O_3 were assumed to be washcoated in the pores of the cordierite substrate. In accordance with experimental data the porosity and average particle size of cordierite substrate in the initial model were 0.5 and 1.0 μm, respectively.

Fig. 9a shows snapshots of CZ particles sintering without cordierite-CZ interaction at 1073 K. The CZ sintering proceeds easily without cordierite-CZ interaction; however the sintering process is considerably suppressed by the presence of the interaction as shown in Fig. 9b. When the temperature is increased to 1273 K, sintering of CZ proceeds much more quickly than at 1073K as shown in Fig. 10a. Even under such a severe condition, as shown in Fig. 10b, the strong interaction of CZ with cordierite surface significantly suppresses the sintering of CZ in cordierite pore. This can also be seen in the results of surface area of CZ at different temperatures shown in Fig. 11. The presence of cordierite-CZ interaction therefore considerably hinders sintering of CZ.

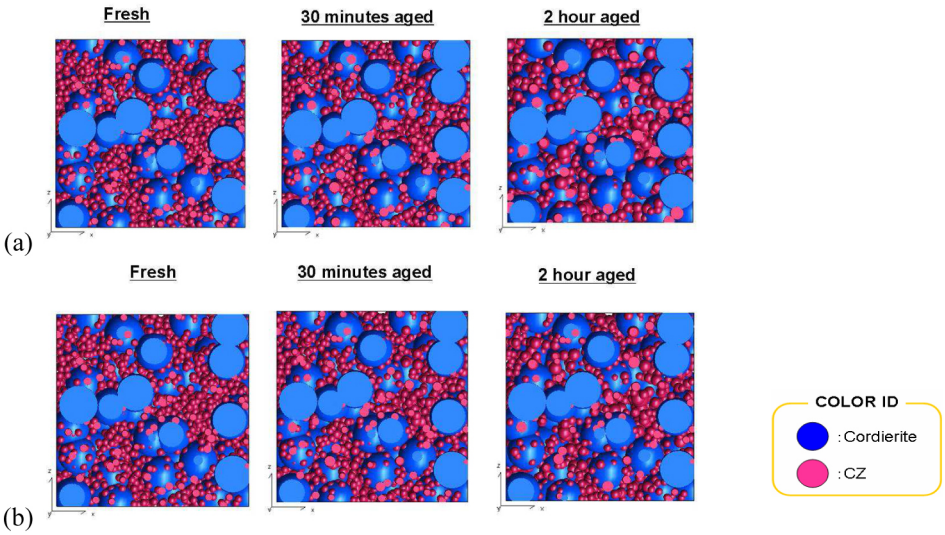

Figure 9. Snapshots of sintering simulation of CZ at 1073 K without, (a), and with, (b), strong interaction of CZ with cordierite.

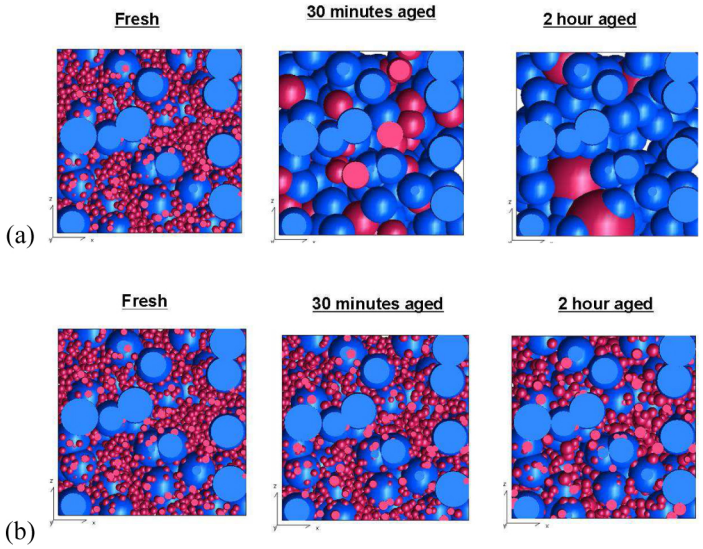

Figure 10. Snapshots of sintering simulation of CZ at 1273 K without, (a), and with, (b), strong interaction of CZ with cordierite.

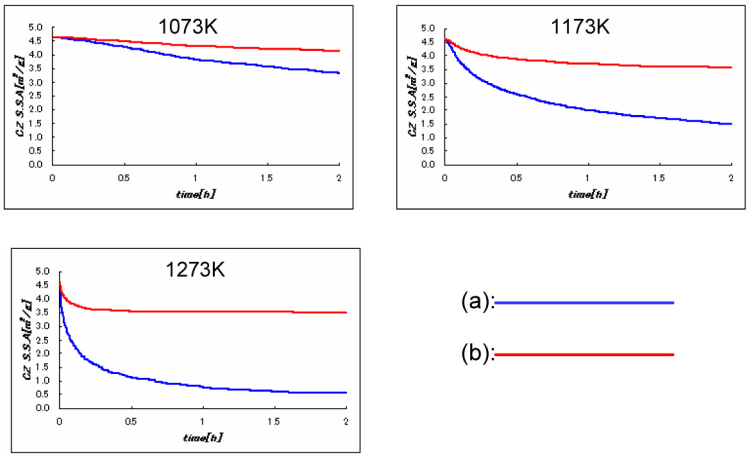

Figure 11. Results of specific surface area change of CZ at various temperatures calculated by SINTA without, (a), and with, (b), strong interaction of CZ with cordierite

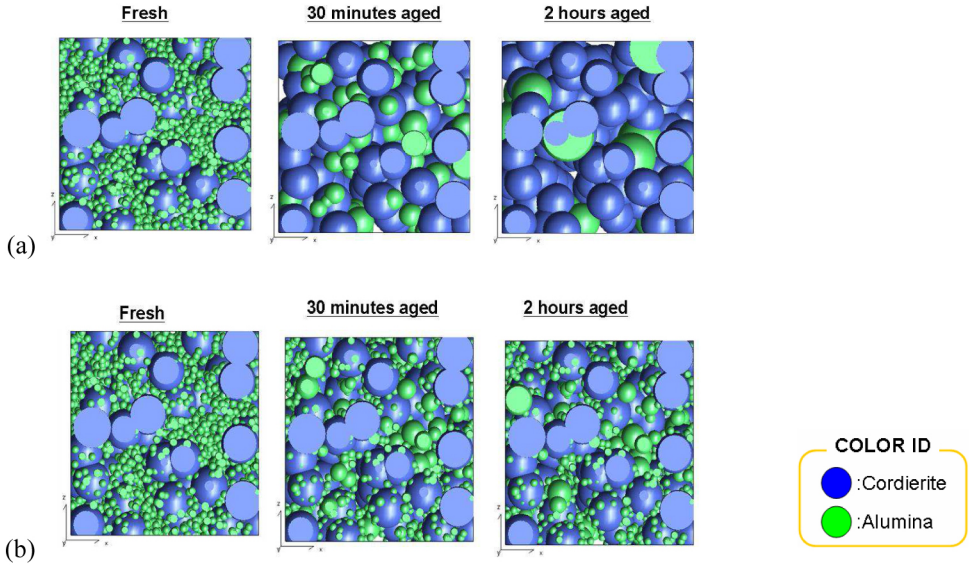

Figure 12. Snapshots of sintering simulation of Al_2O_3 at 1473 K without, (a), and with, (b), strong interaction of Al_2O_3 with cordierite

Similar results are also seen for Al_2O_3 (Fig. 12 and Fig. 13), although sintering here takes place at higher temperatures. As shown in Fig. 12a, sintering of Al_2O_3 proceeds easily at 1473 K when Al_2O_3 particle is not strongly bonded to the cordierite substrate. On the other hand, when Al_2O_3 is strongly bonded as shown in Fig. 12b, sintering is significantly retarded. This can also be seen in the change of specific surface area of Al_2O_3 shown in Fig. 13. The decrease in the specific surface area of Al_2O_3 is greatly suppressed by the presence of strong Al_2O_3-cordierite interaction at any temperature examined.

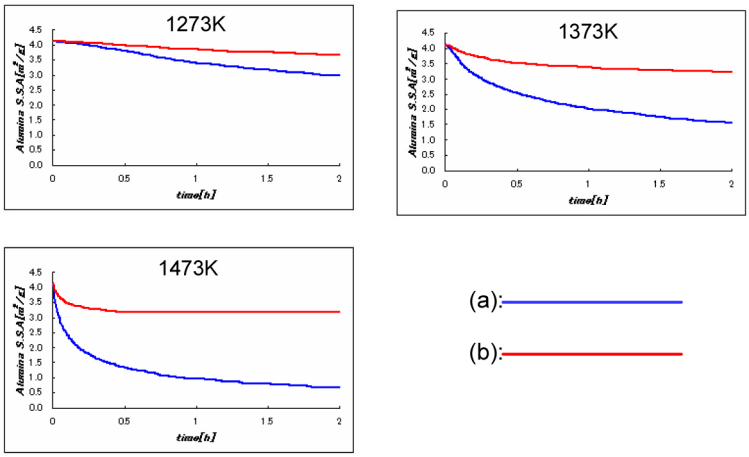

Figure 13. Results of specific surface area change of Al_2O_3 at various temperatures calculated by SINTA without, (a), and with, (b), strong interaction of Al_2O_3 with cordierite.

SUMMARY/CONCLUSIONS

In the present study we have tried to reveal roles of cordierite as a substrate material in automotive catalysts by the application of quantum chemical molecular dynamics technique which takes into consideration both electronic and dynamic effects simultaneously. The results clearly indicate that cordierite has excellent characteristics at various temperatures. It was also shown that cordierite-support interaction was effective in preventing sintering of both CZ and Al_2O_3 supports, further demonstrating the efficacy of cordierite. Since the importance of cordierite-CZ or Al_2O_3 interaction in preventing sintering of CZ or Al_2O_3 did not change significantly with the porosity, the conclusion of the present study is applicable to cordierites with a variety of porosities for a variety of applications such as the substrate of diesel after treatment components and catalytic converters. Further detailed calculations can be done for both applications by using the multi-scale, multi-physics simulators based on the UA-QCMD method.

REFERENCES

1. Suzuki, A., Nakamura, K., Sato, R., Okushi, K., Koyama, M., Tsuboi, H., Hatakeyama, N., Endou, A., Takaba, H., Del Carpio, C.A., Kubo, M., and Miyamoto, A., Topics in Catalysis 52, 1852(2009).

2. Suzuki, A., Nakamura, K., Sato, R., Okushi, K., Tsuboi, H., Hatakeyama, N., Endou, A., Takaba, H., Kubo, M., Williams, M.C., and Miyamoto, A., Surf. Sci. 603, 3049 (2009).

3. Suzuki, A., Sato, R., Nakamura, K., Okushi, K. et al., "Multi-scale Theoretical Study of Sintering Dynamics of Pt for Automotive Catalyst," *SAE Int. J. Fuels Lubr.* 2(2): 337-345, 2010, doi:10.4271/2009-01-2821.

4. Lachman, I. M., Bagley, L.D., Lewis, R.M., Am. Ceram. Soc. Bull, 60, 202-205 (1981).

5. Meille, V., Appl. Catal. A: General 315, 1-17 (2006)

6. Avila, P., Montes, M., and Miro, E. E., Chem. Eng. J. 109, 11-36 (2005).

7. Jiang, P., Lu, G., Guo, Y., Guo, Y., Zhang, S., Wang, X., Surf. Coatings Technol. 190, 314-320 (2005)

8. Hasegawa, J., Ito, M., Itoh, S., and Kondo, T., J. Ceram. Soc. Japan, 113, 626-629 (2005)

9. Hasegawa, J., Ito, M., Itoh, S., and Kondo, T., J. Ceram. Soc. Japan, 114, 199-204 (2006)

10. Alam, M.K., Ahmed, F., Nakamura, K., Suzuki, A., Sahnoun, R., Tsuboi, H., Koyama, M., Hatakeyama, N., Endou, A., Takaba, H., Del Carpio, C.A., Kubo, M., and Miyamoto, A., J. Phys. Chem. C 113, 7723(2009).

11. Ahmed, F., Alam, M.K., Suzuki, A., Koyama, M., Tsuboi, H., Hatakeyama, N., Endou, A., Takaba, H., Del Carpio, C.A., Kubo, M., and Miyamoto, A., J. Phys. Chem. C 113, 15676(2009)

The Engineering Meetings Board has approved this paper for publication. It has successfully completed SAE's peer review process under the supervision of the session organizer. This process requires a minimum of three (3) reviews by industry experts.

ISSN 0148-7191

SAE Customer Service:
Tel: 877-606-7323 (inside USA and Canada)
Tel: 724-776-4970 (outside USA)
Fax: 724-776-0790
Email: CustomerService@sae.org
SAE Web Address: http://www.sae.org
Printed in USA